JACS
JOURNAL OF THE AMERICAN CHEMICAL SOCIETY
Communication
Cite This: J. Am. Chem. Soc. XXXX, XXX, XXX−XXX
pubs.acs.org/JACS

Generalized Synthetic Strategy for Transition-Metal-Doped Brookite-Phase TiO_2 Nanorods

Zhiyong Zhang,[†,#] Qiyuan Wu,[‡,#] Grayson Johnson,[†,#] Yifan Ye,[§] Xing Li,[∥] Na Li,[∥] Meiyang Cui,[†] Jennifer D. Lee,[⊥] Chang Liu,[†] Shen Zhao,[∥] Shuang Li,[∥] Alexander Orlov,[‡] Christopher B. Murray,[⊥] Xu Zhang,[∇] T. Brent Gunnoe,[†] Dong Su,[*,∥] and Sen Zhang[*,†]

[†]Department of Chemistry, University of Virginia, Charlottesville, Virginia 22904, United States
[‡]Department of Materials Science and Chemical Engineering, State University of New York, Stony Brook, New York 11794, United States
[§]Advanced Light Source, Lawrence Berkeley National Laboratory, Berkeley, California 94720, United States
[∥]Center for Functional Nanomaterials, Brookhaven National Laboratory, Upton, New York 11973, United States
[⊥]Department of Chemistry, University of Pennsylvania, Philadelphia, Pennsylvania 19104, United States
[∇]Department of Physics and Astronomy, California State University, Northridge, California 91330, United States

Supporting Information

ABSTRACT: We report a generalized wet-chemical methodology for the synthesis of transition-metal (M)-doped brookite-phase TiO_2 nanorods (NRs) with unprecedented wide-range tunability in dopant composition (M = V, Cr, Mn, Fe, Co, Ni, Cu, Mo, etc.). These quadrangular NRs can selectively expose {210} surface facets, which is induced by their strong affinity for oleylamine stabilizer. This structure is well preserved with variable dopant compositions and concentrations, leading to a diverse library of TiO_2 NRs wherein the dopants in single-atom form are homogeneously distributed in a brookite-phase solid lattice. This synthetic method allows tuning of dopant-dependent properties of TiO_2 nanomaterials for new opportunities in catalysis applications.

Central to functional nanomaterials is the ability to synthetically control nanocrystals physical dimensions, compositions, and structures with atomic-scale precision.[1−7] TiO_2 is one of the most studied metal oxides nanomaterials[8−15] due to its unique semiconducting and oxygen-carrying properties and important applications in optoelectronics,[16] batteries,[17−19] heterogeneous catalysis,[20,21] and photocatalysis.[22−25] For example, TiO_2 can provide active lattice oxygen species and strong interactions with metal nanoparticles, allowing the modulation of kinetics for many heterogeneous catalytic reactions.[26−28] TiO_2 can also absorb photons to generate excited electrons and holes, driving redox reactions for photocatalytic water splitting and photo-reforming processes.[29−32] To maximize the benefits of these applications, an emerging aspect in the studies of TiO_2 nanostructures is to dope them with foreign elements, including cations (e.g., Fe, Sn)[33,34] and/or anions (e.g., C, N, F),[35−39] which can tune lattice oxygen activity as well as improve TiO_2's electronic structure, surface acidity/basicity, and photon absorption, enabling the enhanced catalytic properties.[40−42]

Such a doping strategy has been extensively studied for the rutile- and anatase-phase TiO_2 nanomaterials.[33−36,41] In contrast, brookite TiO_2, another polymorph of TiO_2, is rarely studied due to the challenge of synthesizing the pure brookite phase. Recently, a high-yield synthesis of brookite-phase TiO_2 nanorods (NRs) has been reported via the hydrolysis of titanium chloride precursor,[14] which promoted electron−hole separation under solar irradiation due to the one-dimensional (1-D) structure and therefore delivered a record-high photocatalytic activity toward photo-reforming of ethanol/glycerol for hydrogen (H_2) production.[43] This success for the synthesis of brookite-phase TiO_2 NRs led to the present work, exploring a robust approach to doping for further enhanced catalytic properties. We found that single, dual, or multiple transition-metal (M) dopants in a broad range (M = V, Cr, Mn, Fe, Co, Ni, Cu, Mo, etc., as illustrated in Figure 1) can be homogeneously doped into monodisperse single-crystalline brookite-phase TiO_2 NRs (M-TiO_2). The resultant M-TiO_2 NRs showed consistencies in physical dimensions and surface facets, thereby creating a new class of well-defined TiO_2 nanocrystals with tunable compositions as well as optical and catalytic properties. Using Fe-TiO_2 NRs as a model system, we demonstrated that controlling the Fe-dopant level substantially enhances the photocatalytic performance of TiO_2 brookite-phase nanomaterials.

The M-TiO_2 NRs were synthesized via an organic solution colloidal hydrolysis method {see the Supporting Information (SI)}. Typically, $TiCl_4$ precursor dissolved in oleic acid (OAc) is decomposed in a mixture of 1-octadecene (ODE) and oleylamine (OAm). At high temperature (290 °C), OAm and OAc can react to generate a small amount of water, resulting in slow hydrolysis and condensation of $TiCl_4$ along with the release of HCl. Unlike in the previous method,[43,44] we incorporated M-oleate precursor in our synthesis by mixing it with $TiCl_4$-OAc to produce M-TiO_2. It is known that M-

Received: June 15, 2019
Published: September 19, 2019

DOI: 10.1021/jacs.9b06389
J. Am. Chem. Soc. XXXX, XXX, XXX−XXX

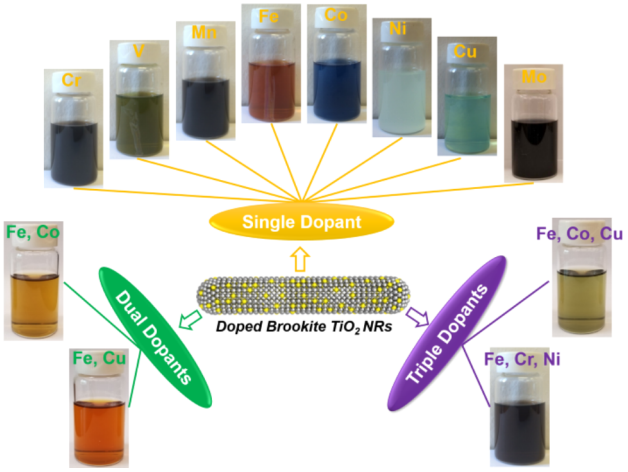

Figure 1. Diverse M-TiO_2 brookite-phase NRs synthesized by the reported synthetic methodology.

oleates, such as Fe-oleate, can be rapidly decomposed to initiate metal oxide nucleation only at temperatures higher than 310 °C.[45] Our reaction temperature (290 °C) and the presence of HCl minimize the possibility of MO_x formation. As a result, M is doped into the TiO_2 matrix, producing M-TiO_2 that can be well-dispersed in nonpolar solvent and exhibit distinct colors relative to undoped TiO_2. As summarized in Figure 1, this strategy can be generalized to all first-row transition-metal dopants and even second-row metals (e.g., Mo) as well as binary and ternary combinations.

Transmission electron microscopy (TEM) and scanning TEM (STEM) images show that the as-synthesized mono-M-TiO_2 (Figures 2A, S1B−G, and S2A), bi-M-TiO_2 (Figure S3), tri-M-TiO_2 (Figure S4), and pristine TiO_2 (Figures S1A and S2B) samples have a consistent NR morphology with an average width of 4.2 ± 0.5 nm and a length of 30−50 nm. These M-TiO_2 NRs preserve the brookite phase, as indicated by their powder X-ray diffraction (XRD) patterns (JCPDS No. 29-1360, orthorhombic), with the characteristic brookite (121) peak at 2θ = 30.81° (Figure S5). By adjusting the precursor M/Ti molar ratio, the M dopant level can be controlled (see SI). TEM images in Figures 2A and S1H confirm that the Fe atomic concentration can be increased up to 10% (out of all cations Fe + Ti, obtained with energy-dispersive X-ray spectroscopy (EDS)) without any obvious morphology change. But we noticed that higher concentrations of M-oleate precursor do not result in further increased doping levels. Instead, M remains in the solution, probably because the stability of the brookite-phase TiO_2 lattice does not favor the incorporation of a high concentration of dopants.

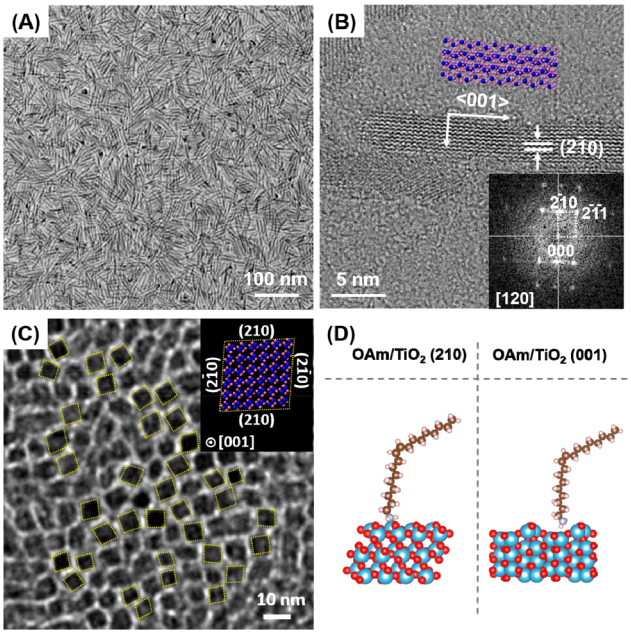

Figure 2. (A) TEM and (B) HRTEM images of the as-synthesized Fe-TiO_2 (10% Fe). (C) TEM image of vertically aligned Fe-TiO_2 (10% Fe) assembly. (D) Optimized OAm adsorption on brookite-phase TiO_2 (210) and (001) planes. Insets in B and C illustrate the corresponding TiO_2 atomic models, with purple and pink atoms being Ti and O, respectively. In the DFT models, the color scheme is red (O), gray (C), white (H), blue (N), and teal (Ti).

High-resolution TEM (HRTEM) images of the representative Fe-TiO_2 (Figure 2B) and pristine TiO_2 NRs (Figure S6) suggest that these NRs are single crystalline and grow along the ⟨001⟩ direction. Fast Fourier transform of HRTEM images in Figure 2B indicates that the side facets might be {210} planes. Thanks to their monodisperse size and morphology, the TiO_2 and Fe-TiO_2 NRs can be easily aligned into ordered assemblies at the interface of air/diethylene glycol via the previous method (Scheme S1).[46] The TEM images (Figures 2C and S7) viewed along the NR longitudinal direction, based on their vertical assemblies, show a rhombic NR cross-section shape with an angle of ∼80°/100°, confirming that the NRs expose four {210} planes as the side facets.

Density functional theory (DFT) calculations (SI) were performed to evaluate the binding between surfactants/ions (OAm, OAc, and Cl^-) and two TiO_2 facets, (001) and (210), to understand the formation mechanism of quadrangular NRs (Figure 2D). We found, in agreement with Gong et al.,[47] that the (001) plane of brookite-phase TiO_2 is not stable and undergoes a 1×1 reconstruction both under vacuum and in the presence of surfactant (Figure S8). Moreover, the adsorption energies (E_{ad}) of OAm, OAc, and Cl^- on the (210) plane were calculated to be −0.93, −0.44, and −0.72 eV, all stronger compared to those on the (001) plane (−0.07, −0.24, and −0.06 eV, respectively) (Table S1). As a result, (210) planes can be preferentially exhibited because of the stronger binding with the surfactants/ions, and such a structure is preserved when only a low concentration of dopant is incorporated. It is worth noting that OAm is present in a much larger amount than OAc and Cl^- in our synthesis and therefore played the most important role in stabilizing the (210) plane due to the strongest E_{ad} (−0.93 eV).

The dopant distribution within NRs was first studied by looking at STEM high-angle annular dark field (HAADF) images coupled with electron energy loss spectroscopy (EELS) elemental mappings (Figures 3A−C and S9−S11). It is clearly seen that the dopants, including Fe mono-dopant, bi-M, and tri-M, are homogeneously distributed within NRs. To further uncover the atomic arrangement and bonding configuration of M, we performed X-ray absorption near-edge structure (XANES) and extended X-ray absorption fine structure (EXAFS) studies. Figure 3D displays the Fe K-edge XANES spectra of Fe-TiO_2 NRs as well as reference samples, including Fe, FeO, Fe_3O_4, and Fe_2O_3. The Fe-TiO_2 spectrum is clearly distinct from those of metallic Fe, excluding the existence of the interstitial dopant of Fe in the TiO_2 lattice. Meanwhile, the

DOI: 10.1021/jacs.9b06389
J. Am. Chem. Soc. XXXX, XXX, XXX−XXX

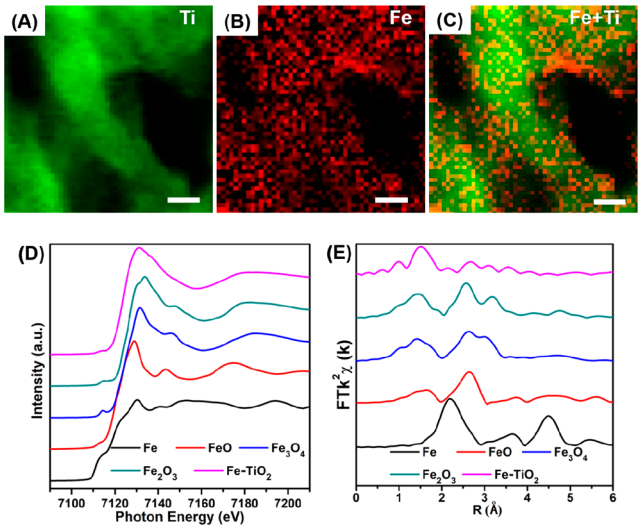

Figure 3. (A–C) HAADF-EELS elemental mappings of Fe-TiO_2 (10%) NRs (scale bar: 2 nm). (D) Fe K-edge XANES and (E) Fourier transform EXAFS spectra of Fe-TiO_2 (10%) and reference standards.

Fe-TiO_2 shows white line characteristics similar to those of FeO_x, indicating the high valence state of Fe (+3) in the Fe-TiO_2 NRs. Additionally, the observed spectra present different profiles in the range of 7120–7160 eV, implying that the state of Fe in Fe-TiO_2 differs from that in FeO_x. We ascribe these differences to the replacement of Fe in the TiO_2 lattice, which is due to the similarity in the ionic radii of Fe^{3+} (0.064 nm) and Ti^{4+} (0.068 nm).[48] Doping of Fe in the TiO_2 lattice alters the hybridization of Fe with O, inducing a different Fe–O bond environment compared with that in FeO_x. Thus, it is clear that Fe is atomically doped into the TiO_2 without forming any FeO_x segregation.

Moreover, the Fe K-edge EXAFS spectrum of Fe-TiO_2 along with the spectra of reference samples are presented in Figure 3E. We found that Fe-TiO_2 does not have the Fe–Fe bond due to the absence of a peak at 2.21 Å, which is an indicator of Fe–Fe bonding observed in metallic Fe foil. Instead, a peak at 1.49 Å, due to the Fe–O bond, is observed in the Fe-TiO_2 spectrum. The peak position is different for FeO (1.57 Å), Fe_3O_4 (1.43 Å), and Fe_2O_3 (1.42 Å). More obviously, the second and third nearest neighboring coordination shells of Fe, in the range of 2–4 eV of Fe-TiO_2, are much weaker compared to those in the FeO_x spectra. This reveals again that the existence of Fe metal and Fe oxide secondary phases in the samples can be excluded, and it indicates that Fe is distributed in the TiO_2 network as single atoms. The EXAFS studies of other M-TiO_2 (Figure S12) also show that single-atom M occupies the Ti site in TiO_2, confirming the universality of atomic doping in the present synthesis.

As illustrated in previous studies on rutile and anatase TiO_2, the t_{2g} state of M dopants can interact with Ti, generating additional occupied states in the bandgap of TiO_2 and tuning the electronic structure of TiO_2.[49] As shown in Figures 1 and S13, our M-TiO_2 NR suspensions in hexanes exhibit different colors from TiO_2 (white), suggesting similar electronic structure modification in brookite-phase TiO_2. The absorption edge of brookite-phase TiO_2 NRs is at ~380 nm in the ultraviolet–visible (UV–vis) diffuse reflectance spectrum (Figure 4A), corresponding to a band gap of ~3.3 eV. For Fe-TiO_2, it can be seen that the Fe dopant shifts the absorption

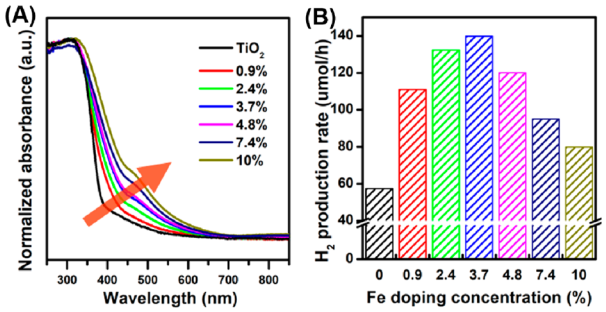

Figure 4. (A) UV–vis diffuse reflectance spectra and (B) photocatalytic H_2 production of TiO_2 and Fe-TiO_2 NRs with different dopant concentrations.

edge of TiO_2 toward longer wavelengths. Therefore, the present synthetic strategy offers an effective method to improve the visible-light absorption of pristine TiO_2 NRs.

To illustrate one potential impact of our general synthesis, we selected the photocatalytic H_2 production via methanol reforming as a model reaction and investigated the performance of Fe-TiO_2 NRs (SI). The pristine TiO_2 brookite-phase NRs, after removal of the surfactants using the $NOBF_4$ treatment[50] and photo-deposition of 1 wt% Pt co-catalyst,[44,51] show a hydrogen production rate of ~57 μmol/h under 300 W xenon lamp illumination (Figure 4B). Interestingly, all the Fe-TiO_2 NRs with different Fe dopant levels show higher H_2 production rates under the same conditions. The H_2 production rate of the 3.7% Fe-TiO_2 reaches ~140 μmol/h, corresponding to a ~2.5 times enhancement compared to that of pristine TiO_2 NRs. Such an enhancement is encouraging, given the fact that the pristine TiO_2 brookite-phase NRs have already been demonstrated as one of the most active photocatalysts.[43,44] Increasing the Fe doping level beyond 3.7% results in decreased activity. The enhanced activity of Fe-TiO_2 probably originates from the improved light utilization in the visible range. However, the dopant atoms can also act as charge recombination sites that compromise the charge separation efficiency, which becomes an issue at higher Fe amounts.[40] Thus, an optimal doping concentration for photocatalytic hydrogen production is observed to be 3.7% Fe. Meanwhile, it was observed that the H_2 production rate decreased only slightly after a 16 h reaction (Figure S14). The Fe-TiO_2 structure and morphology are also well-maintained after catalysis, as indicated by the XRD patterns, TEM images, and EELS elemental mappings (Figures S15 and S16), demonstrating the excellent stability of the Fe-TiO_2 NR photocatalyst.

This Communication highlights a generalized synthetic strategy for doped M-TiO_2 NRs with consistent brookite phase, quadrangular 1-D morphology, and controllable dopant compositions and concentrations. Photocatalytic H_2 production based on the resultant Fe-TiO_2 NRs demonstrates that Fe-doping can lead to a substantial catalytic activity enhancement, probably due to a dopant-induced optical absorption improvement. The unique capability of our synthetic approach in preparing more improved photocatalysts will be further investigated in our follow-up study of M-TiO_2 NRs with diverse M compositions/concentrations. In addition, the present M-TiO_2 NRs may allow additional opportunities in heterogeneous catalysis, serving as a new type of either catalytic materials with single-atom M sites or catalyst supports

DOI: 10.1021/jacs.9b06389
J. Am. Chem. Soc. XXXX, XXX, XXX–XXX

with tunable electronic structure, lattice oxygen activity, and surface acidity/basicity.

■ ASSOCIATED CONTENT

Supporting Information

The Supporting Information is available free of charge on the ACS Publications website at DOI: 10.1021/jacs.9b06389.

Materials and methods, Scheme S1, Table S1, and Figures S1−16 (PDF)

■ AUTHOR INFORMATION

Corresponding Authors

*dsu@bnl.gov

*sz3t@virginia.edu

ORCID

Zhiyong Zhang: 0000-0001-7936-9510

Grayson Johnson: 0000-0001-5229-1135

Jennifer D. Lee: 0000-0003-2644-3507

Xu Zhang: 0000-0002-6491-3234

T. Brent Gunnoe: 0000-0001-5714-3887

Dong Su: 0000-0002-1921-6683

Sen Zhang: 0000-0002-1716-3741

Author Contributions

#Z.Z., Q.W., and G.J. contributed equally to this work.

Notes

The authors declare no competing financial interest.

■ ACKNOWLEDGMENTS

This work was supported by the U.S. National Science Foundation (CBET-1805022). Partial work on electron microscopy was carried out at the Center for Functional Nanomaterials, which is a U.S. Department of Energy Office of Science Facility, at Brookhaven National Laboratory under Contract No. DE-SC0012704. We appreciate experimental support from Sirine Fakra at the Advanced Light Source. The Advanced Light Source is supported by the Director, Office of Science, Office of Basic Energy Sciences, of the U.S. Department of Energy under Contract No. DE-AC02-05CH1123. C.B.M. and J.D.L. acknowledge partial support provided by the Vagelos Institute of Energy Science and Technology at the University of Pennsylvania.

■ REFERENCES

(1) Gilroy, K. D.; Ruditskiy, A.; Peng, H.-C.; Qin, D.; Xia, Y. Bimetallic Nanocrystals: Syntheses, Properties, and Applications. *Chem. Rev.* **2016**, *116*, 10414.

(2) Wu, Y.; Wang, D.; Li, Y. Nanocrystals from Solutions: Catalysts. *Chem. Soc. Rev.* **2014**, *43*, 2112.

(3) Zhou, Z.-Y.; Tian, N.; Li, J.-T.; Broadwell, I.; Sun, S.-G. Nanomaterials of High Surface Energy with Exceptional Properties in Catalysis and Energy Storage. *Chem. Soc. Rev.* **2011**, *40*, 4167.

(4) Cargnello, M.; Gordon, T. R.; Murray, C. B. Solution-Phase Synthesis of Titanium Dioxide Nanoparticles and Nanocrystals. *Chem. Rev.* **2014**, *114*, 9319.

(5) Wang, L.; Holewinski, A.; Wang, C. Prospects of Platinum-Based Nanostructures for the Electrocatalytic Reduction of Oxygen. *ACS Catal.* **2018**, *8*, 9388.

(6) Xia, Y.; Yang, H.; Campbell, C. T. Nanoparticles for Catalysis. *Acc. Chem. Res.* **2013**, *46*, 1671.

(7) Xu, L.; Liang, H.-W.; Yang, Y.; Yu, S.-H. Stability and Reactivity: Positive and Negative Aspects for Nanoparticle Processing. *Chem. Rev.* **2018**, *118*, 3209.

(8) Hahn, R.; Schmidt-Stein, F.; Salonen, J.; Thiemann, S.; Song, Y.; Kunze, J.; Lehto, V.-P.; Schmuki, P. Semimetallic TiO_2 Nanotubes. *Angew. Chem., Int. Ed.* **2009**, *48*, 7236.

(9) Roy, P.; Berger, S.; Schmuki, P. TiO_2 Nanotubes: Synthesis and Applications. *Angew. Chem., Int. Ed.* **2011**, *50*, 2904.

(10) Bai, J.; Zhou, B. Titanium Dioxide Nanomaterials for Sensor Applications. *Chem. Rev.* **2014**, *114*, 10131.

(11) Cargnello, M.; Gordon, T. R.; Murray, C. B. Solution-Phase Synthesis of Titanium Dioxide Nanoparticles and Nanocrystals. *Chem. Rev.* **2014**, *114*, 9319.

(12) Yang, H. G.; Sun, C. H.; Qiao, S. Z.; Zou, J.; Liu, G.; Smith, S. C.; Cheng, H. M.; Lu, G. Q. Anatase TiO_2 Single Crystals with a Large Percentage of Reactive Facets. *Nature* **2008**, *453*, 638.

(13) Gordon, T. R.; Cargnello, M.; Paik, T.; Mangolini, F.; Weber, R. T.; Fornasiero, P.; Murray, C. B. Nonaqueous Synthesis of TiO_2 Nanocrystals Using TiF_4 to Engineer Morphology, Oxygen Vacancy Concentration, and Photocatalytic Activity. *J. Am. Chem. Soc.* **2012**, *134*, 6751.

(14) Buonsanti, R.; Grillo, V.; Carlino, E.; Giannini, C.; Kipp, T.; Cingolani, R.; Cozzoli, P. D. Nonhydrolytic Synthesis of High-Quality Anisotropically Shaped Brookite TiO_2 Nanocrystals. *J. Am. Chem. Soc.* **2008**, *130*, 11223.

(15) Qin, D.-D.; Bi, Y.-P.; Feng, X.-J.; Wang, W.; Barber, G. D.; Wang, T.; Song, Y.-M.; Lu, X.-Q.; Mallouk, T. E. Hydrothermal Growth and Photoelectrochemistry of Highly Oriented, Crystalline Anatase TiO_2 Nanorods on Transparent Conducting Electrodes. *Chem. Mater.* **2015**, *27*, 4180.

(16) Bai, Y.; Mora-Seró, I.; De Angelis, F.; Bisquert, J.; Wang, P. Titanium Dioxide Nanomaterials for Photovoltaic Applications. *Chem. Rev.* **2014**, *114*, 10095.

(17) Gao, X.; Li, G.; Xu, Y.; Hong, Z.; Liang, C.; Lin, Z. TiO_2 Microboxes with Controlled Internal Porosity for High-Performance Lithium Storage. *Angew. Chem., Int. Ed.* **2015**, *54*, 14331.

(18) Yu, X.-Y.; Wu, H. B.; Yu, L.; Ma, F.-X.; Lou, X. W. Rutile TiO_2 Submicroboxes with Superior Lithium Storage Properties. *Angew. Chem., Int. Ed.* **2015**, *54*, 4001.

(19) Singh, D. P.; George, A.; Kumar, R. V.; ten Elshof, J. E.; Wagemaker, M. Nanostructured TiO_2 Anatase Micropatterned Three-Dimensional Electrodes for High-Performance Li-Ion Batteries. *J. Phys. Chem. C* **2013**, *117*, 19809.

(20) Pepin, P. A.; Diroll, B. T.; Choi, H. J.; Murray, C. B.; Vohs, J. M. Thermal and Photochemical Reactions of Methanol, Acetaldehyde, and Acetic Acid on Brookite TiO_2 Nanorods. *J. Phys. Chem. C* **2017**, *121*, 11488.

(21) Enache, D. I.; Edwards, J. K.; Landon, P.; Solsona-Espriu, B.; Carley, A. F.; Herzing, A. A.; Watanabe, M.; Kiely, C. J.; Knight, D. W.; Hutchings, G. J. Solvent-free Oxidation of Primary Alcohols to Aldehydes Using Au-Pd/TiO_2 Catalysts. *Science* **2006**, *311*, 362.

(22) Linsebigler, A. L.; Lu, G.; Yates, J. T. Photocatalysis on TiO_2 Surfaces: Principles, Mechanisms, and Selected Results. *Chem. Rev.* **1995**, *95*, 735.

(23) Wang, C. J.; Thompson, R. L.; Ohodnicki, P.; Baltrus, J.; Matranga, C. Size-dependent photocatalytic reduction of CO_2 with PbS quantum dot sensitized TiO_2 heterostructured photocatalysts. *J. Mater. Chem.* **2011**, *21*, 13452.

(24) Dhakshinamoorthy, A.; Navalon, S.; Corma, A.; Garcia, H. Photocatalytic CO_2 Reduction by TiO_2 and Related Titanium Containing Solids. *Energy Environ. Sci.* **2012**, *5*, 9217.

(25) Hu, J.-L.; Qian, H.-S.; Li, J.-J.; Hu, Y.; Li, Z.-Q.; Yu, S.-H. Synthesis of Mesoporous SiO_2@TiO_2 Core/Shell Nanospheres with Enhanced Photocatalytic Properties. *Part. Part. Syst. Charact.* **2013**, *30*, 306.

(26) Ting, K. W.; Toyao, T.; Siddiki, S. M. A. H.; Shimizu, K.-i. Low-Temperature Hydrogenation of CO_2 to Methanol over Heterogeneous TiO_2-Supported Re Catalysts. *ACS Catal.* **2019**, *9*, 3685.

(27) Widmann, D.; Behm, R. J. Active Oxygen on a Au/TiO_2 Catalyst: Formation, Stability, and CO Oxidation Activity. *Angew. Chem., Int. Ed.* **2011**, *50*, 10241.

DOI: 10.1021/jacs.9b06389
J. Am. Chem. Soc. XXXX, XXX, XXX−XXX

(28) Arrii, S.; Morfin, F.; Renouprez, A. J.; Rousset, J. L. Oxidation of CO on Gold Supported Catalysts Prepared by Laser Vaporization: Direct Evidence of Support Contribution. *J. Am. Chem. Soc.* **2004**, *126*, 1199.
(29) Fujishima, A.; Honda, K. Electrochemical Photolysis of Water at a Semiconductor Electrode. *Nature* **1972**, *238*, 37.
(30) Li, Y. F.; Selloni, A. Pathway of Photocatalytic Oxygen Evolution on Aqueous TiO_2 Anatase and Insights into the Different Activities of Anatase and Rutile. *ACS Catal.* **2016**, *6*, 4769.
(31) Lee, C.-Y.; Park, H. S.; Fontecilla-Camps, J. C.; Reisner, E. Photoelectrochemical H_2 Evolution with a Hydrogenase Immobilized on a TiO_2-Protected Silicon Electrode. *Angew. Chem., Int. Ed.* **2016**, *55*, 5971.
(32) Ni, M.; Leung, M. K. H.; Leung, D. Y. C.; Sumathy, K. A review and recent developments in photocatalytic water-splitting using TiO_2 for hydrogen production. *Renewable Sustainable Energy Rev.* **2007**, *11*, 401.
(33) Choi, W.; Termin, A.; Hoffmann, M. R. The Role of Metal Ion Dopants in Quantum-Sized TiO_2: Correlation between Photoreactivity and Charge Carrier Recombination Dynamics. *J. Phys. Chem.* **1994**, *98*, 13669.
(34) Cao, Y.; He, T.; Chen, Y.; Cao, Y. Fabrication of Rutile TiO_2−Sn/Anatase TiO_2−N Heterostructure and Its Application in Visible-Light Photocatalysis. *J. Phys. Chem. C* **2010**, *114*, 3627.
(35) Dong, F.; Guo, S.; Wang, H.; Li, X.; Wu, Z. Enhancement of the Visible Light Photocatalytic Activity of C-Doped TiO_2 Nanomaterials Prepared by a Green Synthetic Approach. *J. Phys. Chem. C* **2011**, *115*, 13285.
(36) Burda, C.; Lou, Y.; Chen, X.; Samia, A. C. S.; Stout, J.; Gole, J. L. Enhanced Nitrogen Doping in TiO_2 Nanoparticles. *Nano Lett.* **2003**, *3*, 1049.
(37) Yu, J. C.; Yu; Ho; Jiang; Zhang. Effects of F- Doping on the Photocatalytic Activity and Microstructures of Nanocrystalline TiO_2 Powders. *Chem. Mater.* **2002**, *14*, 3808.
(38) In, S.-I.; Vaughn, D. D.; Schaak, R. E. Hybrid CuO-$TiO_{2-x}N_x$ Hollow Nanocubes for Photocatalytic Conversion of CO_2 into Methane under Solar Irradiation. *Angew. Chem., Int. Ed.* **2012**, *51*, 3915.
(39) Xu, L.; Steinmiller, E. M. P.; Skrabalak, S. E. Achieving Synergy with a Potential Photocatalytic Z-Scheme: Synthesis and Evaluation of Nitrogen-Doped TiO_2/SnO_2 Composites. *J. Phys. Chem. C* **2012**, *116*, 871.
(40) Schneider, J.; Matsuoka, M.; Takeuchi, M.; Zhang, J.; Horiuchi, Y.; Anpo, M.; Bahnemann, D. W. Understanding TiO_2 Photocatalysis: Mechanisms and Materials. *Chem. Rev.* **2014**, *114*, 9919.
(41) Liu, B.; Chen, H. M.; Liu, C.; Andrews, S. C.; Hahn, C.; Yang, P. Large-Scale Synthesis of Transition-Metal-Doped TiO_2 Nanowires with Controllable Overpotential. *J. Am. Chem. Soc.* **2013**, *135*, 9995.
(42) Du, Q.; Wu, J.; Yang, H. Pt@Nb-TiO_2 Catalyst Membranes Fabricated by Electrospinning and Atomic Layer Deposition. *ACS Catal.* **2014**, *4*, 144.
(43) Cargnello, M.; Montini, T.; Smolin, S. Y.; Priebe, J. B.; Delgado Jaén, J. J.; Doan-Nguyen, V. V. T.; McKay, I. S.; Schwalbe, J. A.; Pohl, M.-M.; Gordon, T. R.; Lu, Y.; Baxter, J. B.; Brückner, A.; Fornasiero, P.; Murray, C. B. Engineering Titania Nanostructure to Tune and Improve its Photocatalytic Activity. *Proc. Natl. Acad. Sci. U. S. A.* **2016**, *113*, 3966.
(44) Pepin, P. A.; Lee, J. D.; Murray, C. B.; Vohs, J. M. Thermal and Photocatalytic Reactions of Methanol and Acetaldehyde on Pt-Modified Brookite TiO_2 Nanorods. *ACS Catal.* **2018**, *8*, 11834.
(45) Park, J.; An, K.; Hwang, Y.; Park, J.-G.; Noh, H.-J.; Kim, J.-Y.; Park, J.-H.; Hwang, N.-M.; Hyeon, T. Ultra-Large-Scale Syntheses of Monodisperse Nanocrystals. *Nat. Mater.* **2004**, *3*, 891.
(46) Dong, A.; Chen, J.; Vora, P. M.; Kikkawa, J. M.; Murray, C. B. Binary nanocrystal superlattice membranes self-assembled at the liquid−air interface. *Nature* **2010**, *466*, 474.
(47) Gong, X.-Q.; Selloni, A. First-Principles Study of the Structures and Energetics of Stoichiometric Brookite TiO_2 Surfaces. *Phys. Rev. B: Condens. Matter Mater. Phys.* **2007**, *76*, 235307.
(48) Açıkgöz, M.; Gnutek, P.; Rudowicz, C. Modeling Zero-Eield Splitting Parameters for Dopant Mn^{2+} and Fe^{3+} Ions in Anatase TiO_2 Crystal using Superposition Model Analysis. *Chem. Phys. Lett.* **2012**, *524*, 49.
(49) Park, M. S.; Kwon, S. K.; Min, B. I. Electronic Structures of Doped Anatase TiO_2: $Ti_{1-x}M_xO_2$ (M = Co, Mn, Fe, Ni). *Phys. Rev. B: Condens. Matter Mater. Phys.* **2002**, *65*, 161201.
(50) Dong, A.; Ye, X.; Chen, J.; Kang, Y.; Gordon, T.; Kikkawa, J. M.; Murray, C. B. A Generalized Ligand-Exchange Strategy Enabling Sequential Surface Functionalization of Colloidal Nanocrystals. *J. Am. Chem. Soc.* **2011**, *133*, 998.
(51) Wu, Q.; Xiong, S.; Shen, P.; Zhao, S.; Li, Y.; Su, D.; Orlov, A. Exceptional activity of sub-nm Pt clusters on CdS for photocatalytic hydrogen production: a combined experimental and first-principles study. *Catal. Sci. Technol.* **2015**, *5*, 2059.

DOI: 10.1021/jacs.9b06389
J. Am. Chem. Soc. XXXX, XXX, XXX−XXX